Journal of Materials Chemistry A

Accepted Manuscript

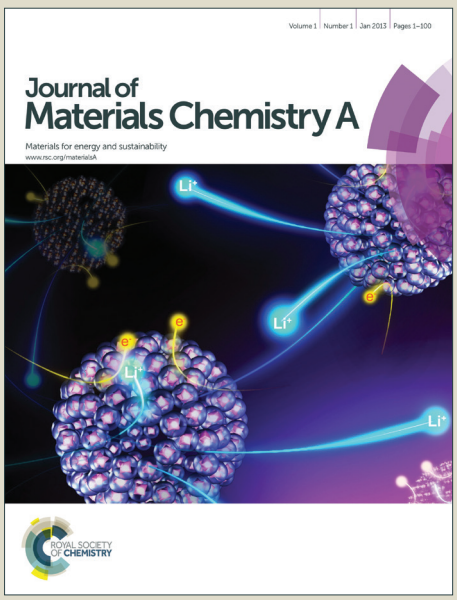

ROYAL SOCIETY OF CHEMISTRY

www.rsc.org/materialsA

Journal Name

RSCPublishing

ARTICLE

In situ coating of nitrogen-doped graphene-like nanosheets on silicon as stable anode for high-performance lithium-ion battery

Cite this: DOI: 10.1039/x0xx00000x

Received 00th XXXXXXXXXX
Accepted 00th XXXXXXXXXX

DOI: 10.1039/x0xx00000x

www.rsc.org/

Hongwei Mi,[a,b] Yongliang Li,[a] Peiyang Zhu,[a] Xiaoyan Chai,[a] Lingna Sun,[a] Haitao Zhuo,[a] Qianling Zhang,[a] Chuanxin He,[*a] Jianhong Liu[*a,b]

Carbon coating is an effective approach to improve the cycling stability of silicon (Si) anode for lithium-ion battery. In this research, we report a facile one-step carbon-thermal method to coat Si nanoparticles with nitrogen-doped (N-doped) graphene-like nanosheets derived from a liquid-polyacrylonitrile (LPAN) precursor. The coated Si anode displays an initial coulombic efficiency of 82%, which is about three times greater than the pristine counterpart, as well as superior cycling stability. The performance improvement is resulting from the conformally coating of the N-doped graphene-like nanosheets, which not only create an electrically conductive network for the electrode, but also provide the buffering matrix to accommodate the volume change of Si during charging and discharging processes.

Introduction

Lithium-ion batteries are one of the most promising energy storage devices for electric vehicles (EVs) or hybrid electric vehicles (HEVs) owing to their relatively high energy density, good cycle life and high power performance.[1,2] However, current graphite anode only has a limited theoretical capacity of 372 mAh·g^{-1}, which will not meet the future energy demand.[2] In order to improve lithium-ion battery performance, alternative anode materials with high capacities and coulombic efficiency are needed.[1, 3] Silicon (Si) is the second most abundant element and comprises 25% of the earth's crust. More importantly, Si has the highest theoretical capacity (4200 mAh·g^{-1} for $Li_{22}Si_5$ at high temperatures[4] or 3579 mAh·g^{-1} for $Li_{15}Si_4$ at room temperature[5,6]) and low working potential (the average delithiation voltage of Si is 0.4 V[4]). However, Si has low electrical conductivity and moreover, the poor cyclability resulted from the large volumetric expansion (>300%) during lithiation and delithiation processes hinders its practical utilization.

In the past decade, many efforts have been devoted to increase the electrochemical performance of Si-based anode. One approach is to minimize Si particles to nanoscale[7] or to prepare nano-structured Si materials, such as Si films[8], Si nanowires[9-13] and Si nanotubes[14], but capacity degradation coupled with electrode fracturing during cycling is still significant. Another method is to mix Si into various carbonaceous materials, such as amorphous carbon[15-20], graphene[21-26], graphite[27,28], carbon nanofibers[29,30], etc. However, the big volume change of Si is only tolerated to a limited degree due to the poor contact between carbon matrix and Si particles, especially during deep charging and discharging process.

Graphene, a two-dimensional monolayer of fused sp^2 carbon bonds in a honeycomb-like network, has received world-wide attention owing to its outstanding properties and potential

applications in the areas of electronics as well as energy conversion and storage devices[31]. Recently, graphene-based composites have shown excellent performance for the advanced lithium-ion batteries due to the high conductivity and large surface area.[32] Luo et al.[22] synthesized crumpled graphene-encapsulated Si nanoparticles by a capillary-driven method from graphene oxide (GO), while Xiang et al.[23] prepared graphene/nanosized-Si composites from GO and graphite. The initial coulombic efficiency of the reduced GO-modified Si anodes in these reports ranged from 55% to 73%. However, the uniformity of the composite is not satisfied because graphene is obtained by chemical reduction from graphene oxide and it is difficult to disperse Si into the solid-state graphene nanosheets. Therefore, it is important to develop an effective route for preparing graphene/Si composites.

Herein, we develop a facile one-step carbon-thermal method to coat Si nanoparticles (hereafter abbreviated as G-Si composite) with nitrogen-doped (N-doped) graphene-like nanosheets (hereafter abbreviated as G) derived from a liquid acrylonitrile homopolymer (LPAN) precursor[33,34] and it is demonstrated that the initial coulombic efficiency of the G-Si composite anode can reach to 82% in average, which is much higher than those of the reduced GO-modified Si anodes. [22-23, 25, 35] To the best of our knowledge, there are few reports on synthesizing graphene/Si composite by using a liquidized polymer as a graphene precursor. The advantage for using LPAN is that it possesses unique fluidic property, which enables LPAN to uniformly coat on Si nanopaticles. In addition, LPAN contains nitrile group and has excellent graphitization ability, which makes it possible to partly transform into N-doped graphene even at 750 ^{o}C.[36] This approach is convenient and low-cost, and is also a rational approach for large-scale production of other alloy-based anode composites for lithium-ion batteries.

Experimental Methods

Preparation of G-Si composites and electrodes

Si (100 nm, Shanghai ST-NANO science & technology Co., Ltd., China) and LPAN with 1:6, 1:10 and 1:14 weight ratio were mixed and ground in a QM-3SP2 planetary ball mill for 10h. The weight ratio of stainless steel (SS) ball to material was maintained at 10:1 and all the millings were carried out at 500 rpm. Then the mixture and pure LPAN were cured in the air at 220 ^{o}C for 3 h and carbonized in argon atmosphere at 800 ^{o}C for 5 h to form G-Si composites and grahene-like nanosheets (G).

Slurries mixed with active materials (Si, G or G-Si), carbon black (CB) and polyvinylidene fluoride (PVDF) in a weight ratio of 7:1:2 were dispersed in n-methyl-2-pyrolidinone (NMP) and spread evenly on a piece of copper (Cu) foil by an automatic film applicator (AFA-II, Shanghai Pushen Chemical Machinery Co., Ltd., China). The coated Cu foil were dried at 60~70 ^{o}C for 12 h and then were cut into □14 mm pieces. Subsequently the pieces were dried at 110 ^{o}C for 6 h in vacuum to be used as electrodes. The loading amount of active material was ~0.6 mg·cm^{-2}. These electrodes were assembled into coin-type 2032 cells (parts obtained from Shenzhen Kejingstar Technology Co., Ltd., China) using a Celgard polypropylene separator, 1 mol·L^{-1} $LiPF_6$/EC:DMC (1:1 by volume) electrolyte, and Li-foil as the counter electrode in an Ar-filled glove box (MBRAUN, Germany) with oxygen and moisture contents less than 0.1 ppm.

Characterization and electrochemical measurements

The thermo-gravimetric analysis was carried out on a STA409PC TG-DSC/DTA instrument (Netzsch, Germany) from 35 to 800 ^{o}C with a heating rate of 10 ^{o}C·min^{-1} in air, from which the contents of Si in the composites were determined. The visual surface topography of the composites were studied by S-3400(Ⅱ) Scanning Electron Microscopy (SEM, Hitachi, Japan) operated at an acceleration voltage of 15 kV. The crystalline structures were obtained by D8 advance X-ray diffraction (XRD, Bruker, Germany) using Cu Kα. X-ray photoelectron spectroscopy (XPS) data were collected with an ESCAlab220i-XL electron spectrometer from VG Scientific

using 300W Al Kα radiation. Transmission electron microscopy (TEM) images were collected on a FEI-Tecnai G2 (USA, 200kV) instrument. Raman measurements were carried out at room temperature using a Jobin Yvon/Atago Bussan T64000 triple spectrometer equipped with micro-optics.

The galvanostatic charge/discharge were carried out on a LAND-CT2001A battery test system (China) between cut-off potentials of 2.00 and 0.01 V at a current density of 200 $mA \cdot g^{-1}$. The electrochemical impedance measurements were accomplished at an AC voltage of 10 mV amplitude by Solartron Impedance analyzer 1260A from 100 kHz to 0.1 Hz.

Results and Discussion

As shown in Scheme 1, the preparation of G-Si composite was accomplished through a facile one-step carbon-thermal assembly. Firstly, Si nanoparticles are uniformly dispersed in LPAN, which is nitrile group containing and low molecular polymer.[33,34] Then the LPAN realigns to the high molecular polymer layer around Si nanoparticles and transition of LPAN is from liquid to solid by stabilization at 220 °C in the air. Finally, LPAN is completely pyrolyzed into N-doped graphene-like nanosheets which conformally coat on the Si nanoparticles at 800 °C. Due to its sheet structure and good mechanical property, the graphene-like nanosheets can prevent the agglomeration of Si nanoparticles and accommodate the volume change of Si particles effectively.

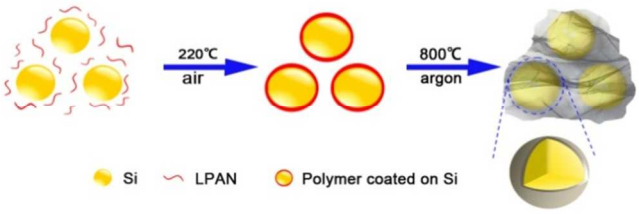

Scheme 1 Schematic illustration of the formation route of G-Si composite.

Structure and Morphology characterization

The Si content in the G-Si composites, determined by TGA in air (Fig. 1), are calculated to be 43 wt%, 29 wt% and 20 wt% for Si: LPAN = 1:6, 1:10, 1:14, respectively. The corresponding G-Si composites are referred as G-43%Si, G-29%Si and G-20%Si, respectively. The initial endothermic peak occurs from 35 to 100 °C, exhibiting a 6 wt% loss attributed to the adsorbed water. The abrupt weight losses occurring between 400 and 690 °C for the G-Si composites indicates the oxidation and decomposition of N-doped graphene-like nanosheets in air.

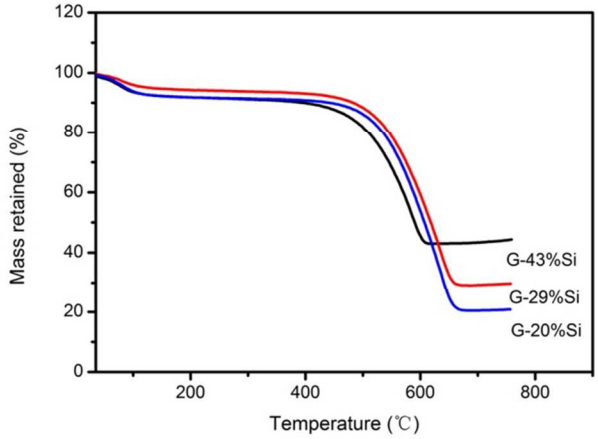

Fig. 1 Thermogravimetric analysis curves of various G-Si composites with different weight ratio of LPAN and Si.

The crystalline structures of Si and G-Si composites were examined by XRD and the patterns are shown in Fig. 2a. All the G-Si composites show a peak at about 26.5°, which corresponds to the C (002) diffraction of graphene-like nanosheets; however, as the Si amount decreases in the composite, the peak intensity increases as well as shifts to a higher degree, indicating more ordered graphene-like nanosheets in the composite. The broad peak at 26.5° suggests that the graphene is homogeneously distributed in the composites without agglomeration.[23] More importantly, the diffraction patterns of Si appear for all G-Si composites, indicating that the Si nanoparticles in the G-Si composites still remain the same crystalline structure during the coating process.

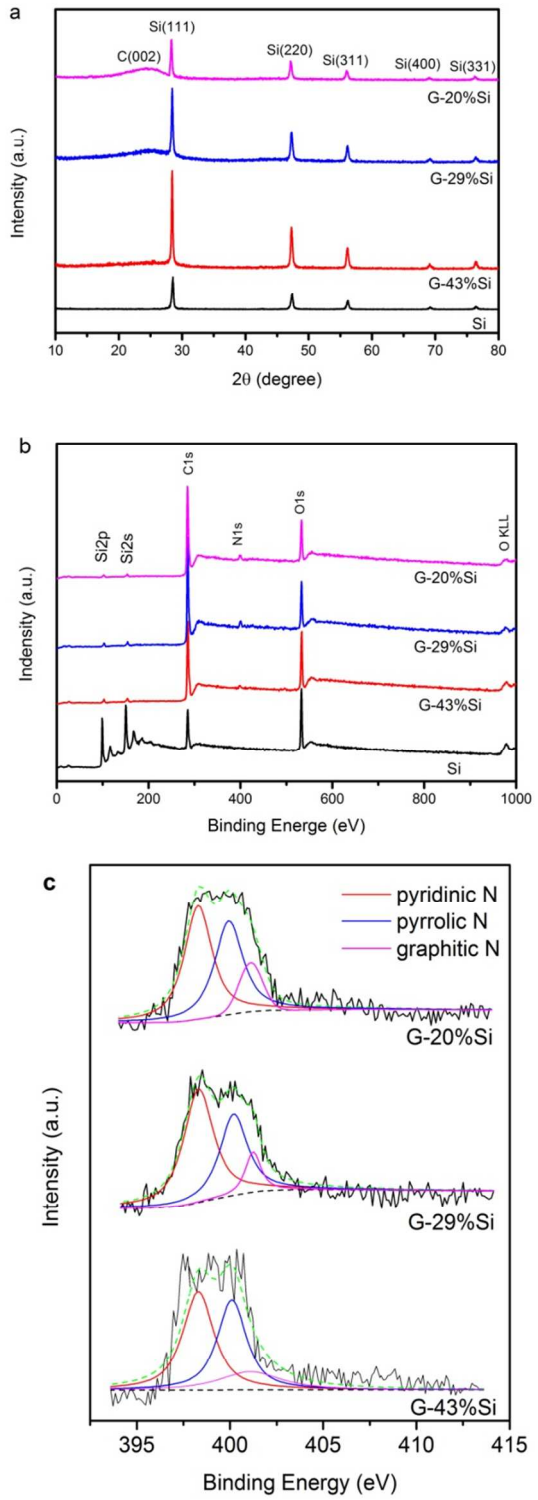

Fig. 2 (a) XRD patterns, (b) XPS spectra of Si, and G-Si composites with different weight ratio of LPAN and Si and (c) XPS N1s spectra of G-Si composites with different weight ratio of LPAN.

X-ray photoelectron spectroscopy (XPS) spectra were used to reveal elemental information of pristine Si and various G-Si composites. Survey scans (Fig. 2b) indicate the existence of C, O, N and Si in the various G-Si composites, while there is no nitrogen in the pristine Si. The intensities of C1s peak for all G-Si composites increase, indicating the presence of graphene-like nanosheets after coating process. Moreover, the graphene-like nanosheets are nitrogen-doped (Fig. 2b) and the N content is 1.9, 3.2 and 3.0 at.% in the G-43%Si, G-29%Si and G-20%Si, respectively. In the N-doped graphene-like nanosheets, the N 1s (Fig. 2c) peak composes of three components: pyridinic N (398.2 eV), pyrrolic N (400.1 eV) and graphitic N (401.7eV). Among these three forms of N binding, the pyridinic N is the most favorable for facilitating the electronic conductivity of the carbon layer and the charge transfer at the interface in Li-ion batteries.[16, 24, 37] The peak intensity for pyridinic N (Fig. 2c) is higher than the other two components, thus the N atoms are mainly in the form of pyridinic N in all three composites.

Raman spectra were employed to indentify the detailed structure of Si and G-Si composites (Fig. 3). As shown in Fig. 3a, the peaks at 1350 and 1580 cm^{-1} correspond to the D and G band of carbon materials, respectively, and the broad peak at around 2600~3100 cm^{-1} is represented as the 2D band of carbon materials.[35, 38, 39] The Raman spectra of all G-Si composites are close to that of single- or bilayer- graphene, which have a lower D peak at 1350 cm^{-1} and a stronger and narrower G peak at 1580 cm^{-1}, and a 2D peak at 2700 cm^{-1}.[38] The broad peak and lower intensity of 2D band indicate the graphene in G-Si composites are several layers. The ratio of intensity between D and G band which represents the defect quantity for G-43%Si, G-29%Si and G-20%Si composites are 0.95, 0.93 and 0.93, respectively. In Fig. 3b, commercial Si nanoparticles show a peak at 515 cm^{-1}, while G-Si composites show a lower intensity and downshift band at 509 cm^{-1}. Our observation is similar to

the previously reports, [39, 40] which ascribed to the transverse optical mode, demonstrating the Si nanoparticles coated by the thin carbon layers.

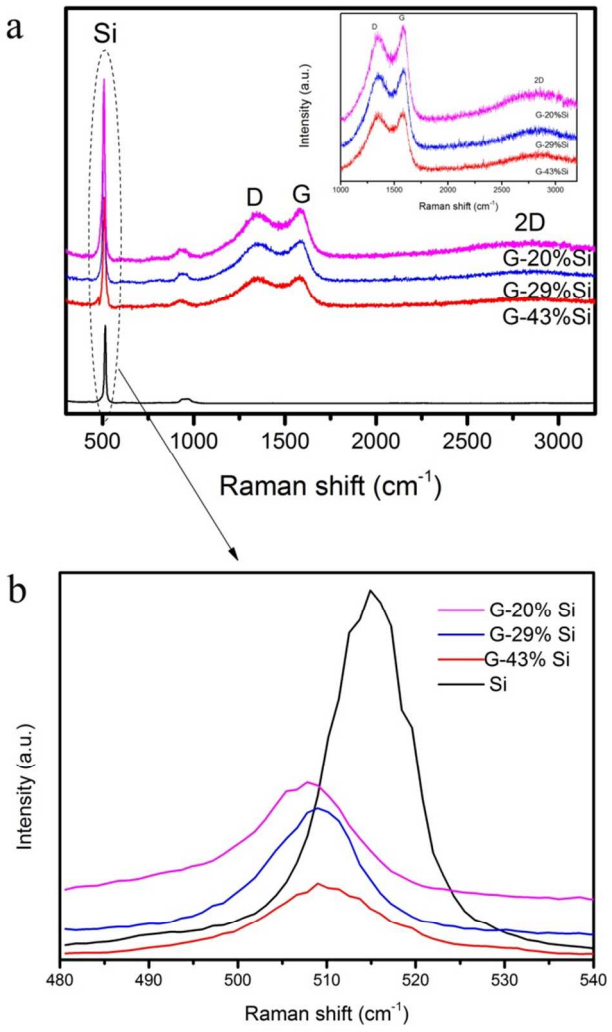

Fig. 3 (a) Raman spectra of Si and G-Si composites with different weight ratio of LPAN and Si and (b) Magnified view of peaks marked in the image (a), indicating the downshift of G-Si composites bands.

The morphology of Si and G-Si composites were observed by SEM and TEM. It is clear that the particle size of Si is at nanometer scale and Si nanoparticles are homogeneously encapsulated by uniform N-doped graphene-like nanosheets after coating (Fig. 2b, Fig. S1 and Fig. 4). There are many poles in G-Si composites (Fig. S1c and d, Supplementary Information), which can provide void space to accommodate the volume change of Si during discharge/charge cycles. The void space might be caused by some small molecules (such as NH_3, CO etc) spilling out during stabilization at 220 ^oC and carbonization reaction. Moreover, the TEM images of G-Si composites (Fig. 4) show that the core nanoparticles are well-wrapped within the outer graphene-like matrix and the observed lattice fringes in the core region with a lattice spacing of 0.31 nm originates from the Si (111) planes. The Si nanoparticles are separated from each other and there are spaces among particles. As shown in the high resolution TEM image (Fig. 4b), the thickness of the graphene-like layer of G-43%Si composite is about 3-4 nm, while the thickness of the other two composites are 5-8 nm (Fig. 4d and Fig. 4f).

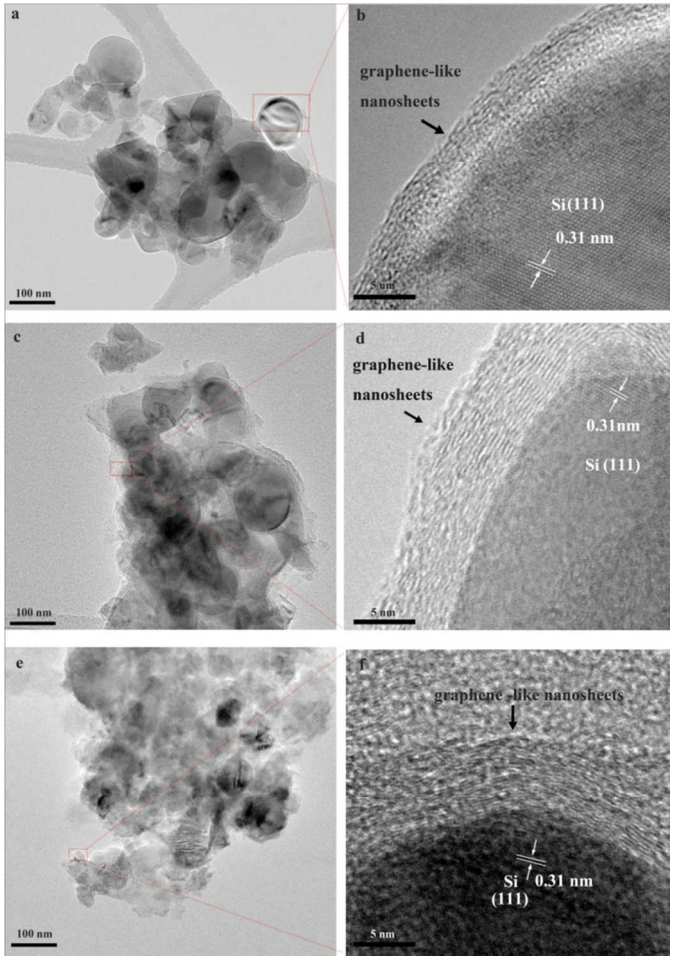

Fig. 4 TEM image of (a), (b) G-43% Si composite, (c), (d) G-29% Si composite and (e), (f) G-20% Si composite.

Electrochemical performance

The electrochemical performance of G-Si composites and Si nanoparticles as anodes for lithium-ion batteries were evaluated using galvanostatic charge/discharge cycles at 200 mA·g^{-1} between 0.01 and 2 V. Fig. 5 shows the initial charge/discharge curves of Si and G-Si composites. All samples show a voltage plateau at ~0.4 V for charging which is due to the unique feature of Si-based electrodes. During discharge, the long flat plateau at ~0.1 V is indicative of the alloying reaction between crystalline Si and Li.[41] The first charge specific capacities of G-43% Si, G-29% Si and G-20% Si composites were 1533, 1085 and 1022 mAh·g^{-1}, while the initial coulombic efficiencies of three composites were 82.4%, 82.2% and 83.9%, respectively. The initial coulombic efficiency of G-Si composites are three times greater than that of Si nanoparticles (only 28.7%), which indicates a conformal coating for Si nanoparticles by N-doped graphene-like nanosheets that protects Si nanoparticles from electrolyte solvents.

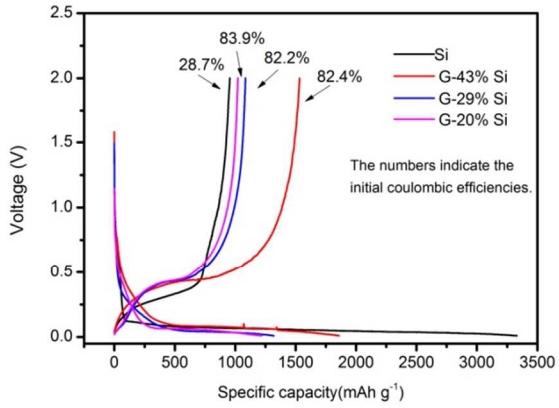

Fig. 5 Initial charge-discharge voltage profiles of the cells with various G-Si composites as well as the Si anode. The numbers indicate the initial coulombic efficiencies.

The variation of specific gravimetric capacity with cycle number of Si, the graphene-like nanosheets and G-Si composite anodes are shown in Fig. 6. After 50 cycles, the reversible capacity at a current density of 200mA·g^{-1} is 341 mAh·g^{-1} for gaphene-like nanoshents (45% retention of the initial capacity), which is similar to the performance of graphene nanosheet reported by Yoo's group.[42] The discharge capacity of Si nanoparticles quickly decreases from 3329.9 to 2.9 mAh·g^{-1} after 6 cycles (Fig. 6). This would be attributed to the poor intrinsic electrical conductivity and dramatic destruction of initial morphology of Si nanoparticles during Li insertion/extraction, leading to the loss of electrical contact between active materials and the electrode framework. However, the anode made of G-29%Si composite demonstrated superior charge/discharge capacities and cycle performances. The initial discharge capacity was 1319 mAh·g^{-1} and the capacity was 819 mAh·g^{-1} after 50 cycles, while for G-43% Si composite, the capacity decreased to 478 mAh·g^{-1} after 30 cycles. The reversible retention capacity after 50 cycles was 18, 62 and 55% for G-43% Si, G-29% Si and G-20% Si composite, respectively. Indeed, as shown in Fig. S2 (Supplementary Information), the TEM images of composites after 50 electrochemical cycles confirmed that Si nanoparticles are uniformly distributed on graphene-like networks in G-29% Si and G-20% Si composites, while some Si nanoparticles are not wrapped by graphene-like nanosheets in G-43% Si composite.

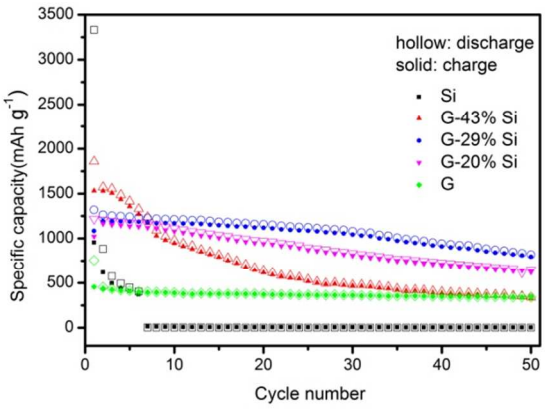

Fig. 6 Cycling performance of various G-Si composite anodes compared to Si and graphene-like nanosheets anode at a current density of 200 mA·g^{-1}.

The coulombic efficiency of G-29%Si composite reached to 97% after two cycles and remained relatively stable in subsequent cycles (Fig. 7a). Moreover, the G-29%Si composite anode was further tested at various step-wise current densities. The cells were tested to charge/discharge cycling from 200 mA·g^{-1} to 10 A·g^{-1} and then reversed to 200 mA·g^{-1} (Fig 7b). The specific capacities of 829 and 601 mAh·g^{-1} can be achieved even at high current densities of

2 A·g^{-1} and 4 A·g^{-1}. The capacity recovers to 1128 mAh·g^{-1} when the current density is restored to 200 mA·g^{-1}, which indicate that the integrity of G-29%Si composite anode was maintained. The excellent cycle performance as well as extremely high initial coulombic efficiency of the G-Si composite are mainly attributed to the following reasons: firstly, the graphene-like nanosheets provide the electrode with more flexibility as well as electrical contact, and protect the electrode from cracking; secondly, the graphene-like nanosheets can prevent the agglomeration of Si nanoparticles and accommodate the volume change of Si particles effectively due to its sheet structure and good mechanical property; thirdly, G-Si composites provide void space, which is formed during carbonization, to meet the volume change of Si during discharge/charge.

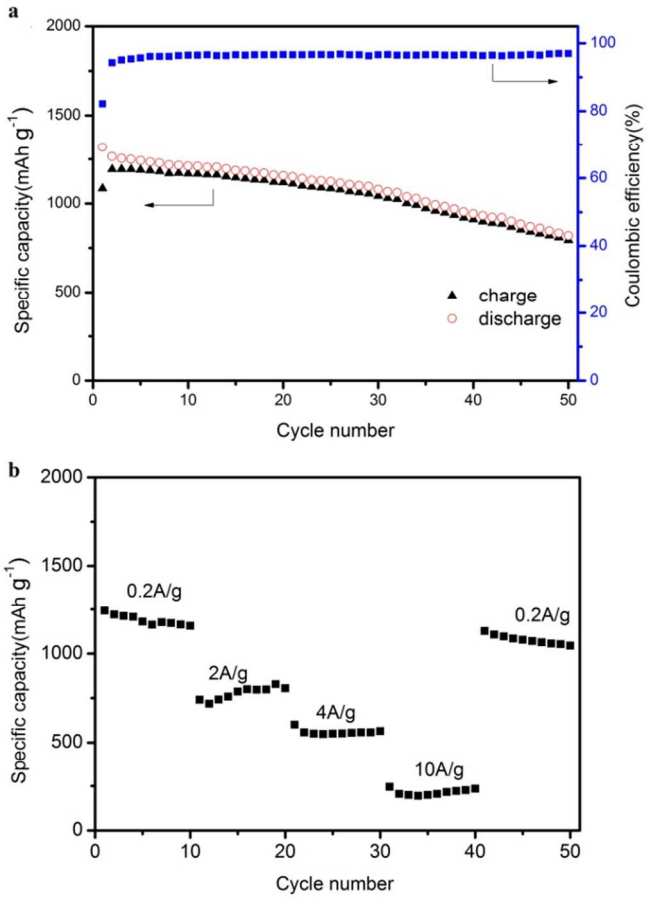

Fig. 7 (a) Cycling performance and coulombic efficiency and (b) Rate performance of G-29%Si composite anode.

Fig. 8 shows the EIS of the various G-Si composites as well as the Si anode after 50 cycles. All cells exhibit a semicircle over the high frequency range, followed by a straight line in the low frequency region. Large semicircles observed for Si electrode is indicative of high interfacial charge-transfer resistance (R_{ct}),[23] which can be attributed to the poor electrical conductivity of Si nanoparticles. The diameter of the semicircle for the G-Si composites electrode is smaller than that of Si electrode, indicating that G-Si composite electrodes possess lower resistance, which is due to the stable structure and the improved conductivity by the uniform coating of N-doped graphene-like nanosheets on Si. Compared to the G-43%Si composite, the R_{ct} of the other two composites are lower, indicating they have higher electric conductivity than G-43%Si composite anode.

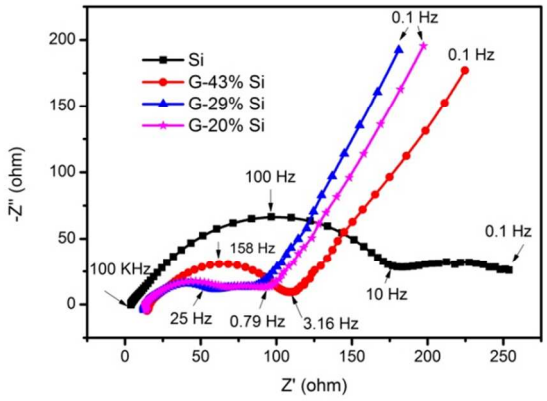

Fig. 8 EIS of the various G-Si composite anodes as well as the Si anode.

Conclusions

In conclusion, we have developed a facile one-step carbon-thermal method to conformally coat Si nanoparticles with N-doped graphene-like nanosheets. In terms of cycling stability and coulombic efficiency, the G-Si composites possess good electrochemical performance than those of Si nanoparticles. In particular, the coulombic efficiency of G-29%Si composites can at least reach to 82.2% in the first charge/discharge cycle, while the discharge capacity remains 819 mAh·g^{-1} after 50 cycles at 200 mA·g^{-}

[1]. Excellent performance of G-Si composites can be attributed to the following reasons: the N-doped graphene-like nanosheets provide the electrode with more flexibility as well as electrical contact, and protect the electrode from cracking; the graphene-like nanosheets can prevent the agglomeration of Si nanoparticles and accommodate the volume change of Si particles effectively due to its sheet structure and good mechanical property; and G-Si composites provide void space, which is formed during carbonization, to meet the volume change of Si during discharge/charge. This approach is convenient and low-cost, and also a suitable approach for large-scale production of other alloy-based anode composites for lithium-ion batteries.

Acknowledgements

This work is financially supported by the Natural Science Found Council of China (No. 21001074), Foundation for Emerging Industries of Strategic Importance of Shenzhen (No.CXZZ20120830160459755 and No. ZDSY20120612094546592), Major Programs for Science and Technology Development of Shenzhen (No. XCL201110060) and Major Programs on Basic Research of Shenzhen (No. JC201104210008A). The TEM used in this work was supported by the Institute for Advanced materials (IAM) with funding from the special Equipment Grant from the University Grants Committee of the Hong Kong Special Administrative Region, China (SEG_HKBU06). Benson Leung and Ke Li are greatly acknowledged for the convenience of material characterization.

Notes and references

[a] Shenzhen Key Laboratory of Functional Polymer, College of Chemistry and Chemical Engineering, Shenzhen University, Shenzhen, 518060, PR China. Tel/Fax: +86-755-26536141; E-mail: Liujh@szu.edu.cn.

[b] Faculty of Material and Chemical Engineering, China University of Geosciences Wuhan, 430074, PR China.

1. J. M. Tarascon and M. Armand, *Nature*, 2001, **414**, 359.
2. M. Armand and J. M. Tarascon, *Nature*, 2008, **451**, 652.
3. M. L. Terranova, S. Orianducci, E. Tamburri, V. Guglielmotti and M. Rossi, *J. Power Sources*, 2014, **246**, 167.
4. H. Wu and Y. Cui, *Nano. Today*, 2012, **7**, 414.
5. M. N. Obrovac and L. Christensen, *Electrochem. Solid-State Lett.*, 2004, **7**, A93.
6. X. H. Liu, L. Q. Zhang, L. Zhong, Y. Liu, H. Zheng, J. W. Wang, J.-H. Cho, S. A. Dayeh, S. T. Picraux, J. P. Sullivan, S. X. Mao, Z. Z. Ye and J. Y. Huang, *Nano. Lett.*, 2011, **11**, 2251.
7. H. Kim, M. Seo, M.-H. Park and J. Cho, *Angew. Chem. Int. Ed.*, 2010,**49**, 2146.
8. S. Oharaa, J. Suzuki, K. Sekinea and T. Takamura, *J. Power Sources*, 2004, **136**, 303.
9. V. Etacheri, O. Haik, Y. Goffer, G. A. Roberts, I. C. Stefan, R. Fasching and D. Aurbach, *Langmuir.*, 2012 **28**, 965.
10. C. K. Chan, H. Peng, G. Liu, K. Mcllwrath, X. F. Zhang, R. A. Huggins and Y. Cui, *Nat. Nanotech.*, 2008. **3**, 31.
11. N. Liu, L. B. Hu, M. T. McDowell, A. Jackson and Y. Cui, *ACS Nano*, 2011, **5**, 6487.
12. L. F. Cui, R. Ruffo, C. K. Chan, H. L. Peng and Y. Cui, *Nano Lett.*, 2009, **9**, 491.
13. H. T. Nguyen, F. Yao, M. R. Zamfir, C. Biswas, K. P. So, Y. H. Lee, S. M. Kim, S. N. Cha, J. M. Kim and D. Pribat, *Adv. Energy Mater.*, 2011, **1**, 1154.
14. W. J. Lee, M. H. Park, Y. Wang, J. Y. Lee and J. Cho, *Chem. Commun.*, 2010, **46**, 622.
15. J. Guo, Z. Yang and L. A. Archer, *J. Mater. Chem. A,* 2013,**1**, 5709.
16. N. Liu, H. Wu, M. T. McDowell, Y. Yao, C. Wang and Y. Cui, *Nano Lett.*, 2012, **12**, 3315.
17. Y. Hwa, W. S. Kim, S. H. Hong and H. J. Sohn, *Electrochim. Acta*, 2012, **71**, 201.
18. S. Chen, M. L. Gordin, R. Yi, G. Howlett, H. Sohn and D. H. Wang, *Phys. Chem. Chem. Phys.*, 2012, **14**, 12741.
19. R. Yi, F. Dai, M. L. Gordin, S. R. Chen and D. H. Wang, *Adv. Energy Mater.*, 2013, **3** , 295.
20. B.-S. Lee, S.-B. Son, K.-M. Park, J.-H. Seo, S.-H. Lee, I.-S. Choi, K.-H. Oh and W.-R. Yu, *J. Power Sources*, 2012, **206**, 267.

21. X. Zhao, C. M. Hayner, M. C. Kung and H. H. Kung, *Adv. Energy Mater*. 2011, **1**, 1079.

22. J. Luo, X. Zhao, J. Wu, H. D. Jang, H. H. Kung and J. Huang, *J. Phys. Chem. Lett*. , 2012, **3**, 1824.

23. H. Xiang, K. Zhang, G. Ji, J. Y. Lee, C. Zou, X. Chen and J. Wu, *Carbon*, 2011, **49**, 1787.

24. R. C. Guzman, J. H. Yang, M. M. Cheng, S. O. Salley and K.Y. Ng, *J. Power Sources*, 2014, **246**, 335.

25. L. Zhang, W. Hao, L. Zhang, X. Feng, Y. Zhang, W. Chen, H. Pang and H. Zheng, *J. Mater. Chem. A*, 2013, **1**, 7601.

26. Y. Wen, Y. J. Zhu, A. Langrock, A. Manivannan, S. H. Ehrman and C. S. Wang, Small, 2013, **9**, 2810.

27. Y. Chen, J. Qian, Y. Cao, H. Yang and X. Ai, *ACS Appl. Mater. Interfaces*, 2012, **4**, 3753.

28. C.-H. Yim, F. M. Courtel and Y. Abu-lebdeh, *J. Mater. Chem. A,* 2013, **1**, 8234.

29. Y. Li, B. K. Guo, L. W. Ji, Z. Lin, G. J. Xu, Y. Z. Liang, S. Zhang, O. Toprakci, Y. Hu, M. Alcoutlabi and X. W. Zhang, *Carbon*, 2013, **51**, 185.

30. S. A. Klankowski, R. A. Rojeski, B. A. Cruden, J. Liu, J. Wu and J. Li, *J. Mater. Chem. A*, 2013, **1**, 1055.

31. D. C. Wei and Y. Q. Liu, *Adv. Mater.* 2010, **22**, 3225.

32. Y. Q. Sun, Q. Wu and G. Q. Shi, *Eenrgy Environ. Sci.,* 2011, **4**, 1113.

33. J. H. Liu, D. Y. Gui, Q. L. Zhang, C. X. He and C. Z. Zhu, *PCT Patent*, 2012, WO/2012/089085.

34. J. H. Liu, J. Xu, S. Q. Wu, Q. L. Zhang, C. X. He and C. Z. Zhu, *CN Patent*, 2011, 201110086492.

35. M. Zhou, T. W. Cai, F. Pu, H. Chen, Z. Wang, H. Y. Zhang and S. Y. Guan. *ACS Appl. Mater. Interfaces*, 2013, **5**, 3449.

36. H. T. Zhuo, S. Wan, C. X. He, Q. L. Zhang, C. H. Li, D.Y. Gui, C. Z. Zhu, H. B. Niu and J. H. Liu, *J. Power Sources*, 2014, **247**, 721-728.

37. L. Zhao, Y. S. Hu, H. Li, Z. X. Wang and L. Q. Chen. *Adv. Mater*. 2011, **23**,1385.

38. L. J. Ci, L. Song, C. H. Jin, D. Jariwala, D. X. Wu, Y. J. Li, A. Srivastava, Z. F. Wang, K. Storr, L. Balicas, F. Liu and P. M. Ajayan, *Nat. Mater.* , 2010, **9**, 430.

39. D. C. Wei, Y.Q. Liu, Y. Wang, H. L. Zhang, L. P. Huang and G. Yu, *Nano. Lett*. , 2009, **9**, 1752.

40. S. Q, Chen, P. T. Bao, X. D. Huang, B. Sun, G. X. Wang, Nano Res., 2014, **7**, 85.

41. L. F. Cui, Y. Yang and C. M. Hsu, Nano Lett., 2009, **9**, 3370.

42. E. J. Yoo, J. Kim, E. Hosono, H. S. Zhou, T. Kudo and I. Honma, *Nano. Lett* .,2008, **8**, 2277.

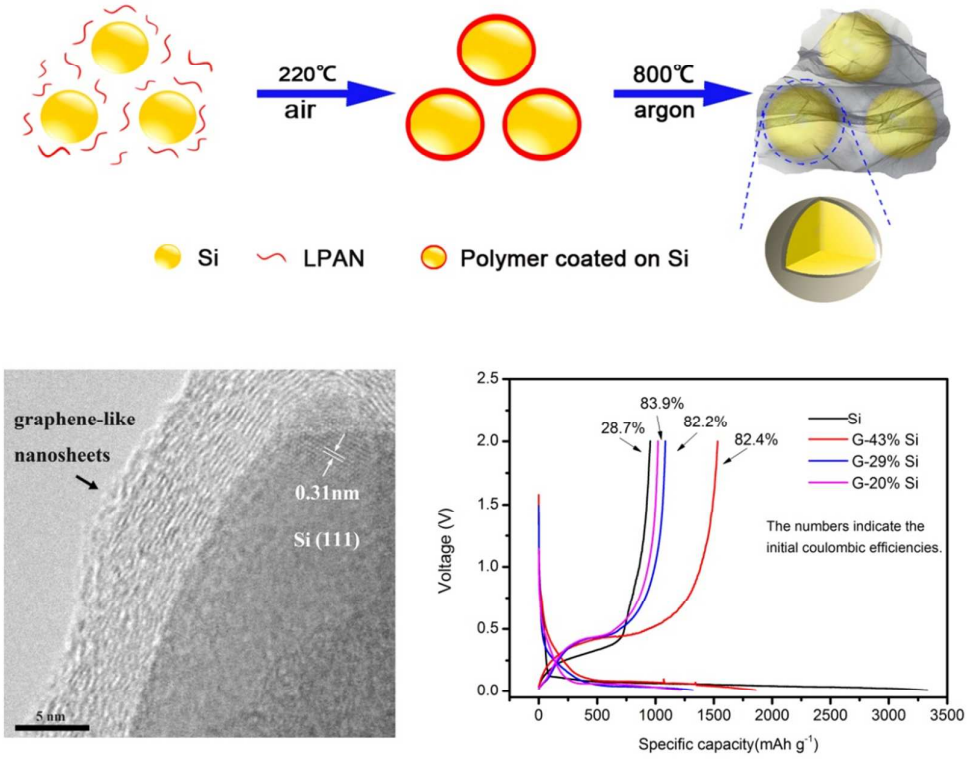

Si nanoparticles are coated with nitrogen-doped graphene-like nanosheets by a facile one-step carbon-thermal method, and the coated Si anode displays high initial coulombic efficiency.